AGU ADVANCING EARTH AND SPACE SCIENCES

Geophysical Research Letters®

RESEARCH LETTER
10.1029/2024GL111428

Detecting Millimetric Slow Slip Events Along the North Anatolian Fault With GNSS

Alpay Özdemir[1], Jorge Jara[2], Uğur Doğan[3], Romain Jolivet[4,5], Ziyadin Çakir[6], Jean-Mathieu Nocquet[7,8], Semih Ergintav[9], and Roger Bilham[10]

[1]Engineering Faculty, Department of Civil Engineering, Adiyaman University, Adiyaman, Türkiye, [2]GFZ Helmholtz Centre for Geosciences, Potsdam, Germany, [3]Faculty of Civil Engineering, Department of Geomatic Engineering, Yildiz Technical University, Istanbul, Türkiye, [4]Laboratoire de Géologie, Département de Géosciences, UMR 8538, École Normale Supérieure, PSL Université, Paris, France, [5]Institut Universitaire de France, Paris, France, [6]Department of Geological Engineering, Istanbul Technical University (ITU), Istanbul, Türkiye, [7]Université Côte d'Azur, IRD, CNRS, Observatoire de la Côte d'Azur, Géoazur, Valbonne, France, [8]Université Paris Cité, Institut de Physique du Globe de Paris, Paris, France, [9]Department of Geodesy, Kandilli Observatory and Earthquake Research Institute, Bogazici University, Istanbul, Türkiye, [10]CIRES and Geological Sciences, University of Colorado, Boulder, CO, USA

Key Points:

- We propose a strategy combining geodetic reference frame definition and time series analysis to extract slow slip events from GNSS data
- We detect and characterize a shallow, 10-km-long, three-week-long slow slip event along the central section of the North Anatolian Fault
- We show that persistent aseismic slip and slow slip events are spatially complementary and interact at shallow depth

Supporting Information:

Supporting Information may be found in the online version of this article.

Correspondence to:

J. Jara,
jorge@gfz.de

Citation:

Özdemir, A., Jara, J., Doğan, U., Jolivet, R., Çakir, Z., Nocquet, J.-M., et al. (2025). Detecting millimetric slow slip events along the North Anatolian Fault with GNSS. *Geophysical Research Letters*, *52*, e2024GL111428. https://doi.org/10.1029/2024GL111428

Received 29 JUL 2024
Accepted 11 MAR 2025

Abstract Active faults release part of the elastic strain energy stored in the crust via aseismic slip, either through slow slip events (SSEs) or steady slowly creep. However, spatial and temporal interactions between these different styles of aseismic slip have yet to be quantified especially at depth. Along the central section of the North Anatolian Fault, we apply a Multichannel Singular Spectrum Analysis (MSSA) on GNSS time series of ground motion to detect a M_w 4.8 ± 0.08 shallow SSE (2–5 km depth) lasting for 26 ± 5 days, in agreement with local creepmeter observations. Our observations confirm the recurrence of SSEs next to a steadily creeping section of the fault. Finally, we discuss how steady creep and SSEs interact spatially and temporally along the fault segment.

Plain Language Summary Tectonic strain on most active faults is typically released violently in earthquakes. However, some faults slip slowly, releasing strain either steadily (steady creep) or in sudden, short-term bursts called slow slip events (SSEs). On the North Anatolian Fault near Ismetpasa, Türkiye, slip occurs both in large earthquakes, like the 1944 Bolu earthquake (Magnitude 7.4), and as continuous slow slip in the shallow crust, interrupted by occasional SSEs. At the end of 2019, we detected a significant SSE lasting four weeks with over 7 mm of surface slip. This event was recorded by five displacement sensors (creepmeters) across a 4.9-km fault segment and by five GNSS sensors spanning about 80 km. Our analysis shows that the slip, equivalent to a Magnitude 4.8 earthquake, extended up to 10 km deep, with most slip concentrated within a 5 × 5 km patch west of Ismetpasa. This study advances our understanding of how faults release tectonic stresses, which is valuable for improving earthquake hazard assessments.

1. Introduction

Since the 1960s, aseismic slip has emerged as a critical aspect of the earthquake cycle, challenging Reid's theory that only earthquakes release accumulated elastic energy (Reid, 1910). It is now understood that aseismic slip occurs during all stages of the earthquake cycle via various mechanisms, such as afterslip (Bürgmann et al., 2001; Heki et al., 1997; Hsu et al., 2002), earthquake triggering (Ruiz et al., 2014; Radiguet et al., 2016; Socquet et al., 2017; N. Voss et al., 2018), interseismic SSEs (burst-like behavior) (Avouac, 2015; Bürgmann, 2018; Jolivet & Frank, 2020, and references therein), steady-state creep (Ambraseys, 1970; Cakir et al., 2005; Dalaison et al., 2021; Jolivet et al., 2015; Jolivet, Jara, Dalaison, et al., 2023; Louderback, 1942; Steinbrugge et al., 1960), or spatial variations in interseismic geodetic coupling (Bürgmann et al., 2005; Jara et al., 2017, 2024; Materna et al., 2019; Mazzotti et al., 2000; Schurr et al., 2014). Most SSE descriptions come from subduction zones, where land-based observations limit detailed mapping of these phenomena. Some SSEs have been detected along continental faults, but the fine relationship with persistent aseismic slip remains underexplored (e.g., Murray & Segall, 2005). Further investigation into the relationship between SSEs and regions of long-term creep could benefit from high-resolution descriptions. Here, we present a methodology to detect and characterize SSEs along continental strike-slip faults and explore interactions between aseismic slip modes.

The central section of the North Anatolian Fault Zone (NAFZ) is an excellent place to study such interactions. The region was struck in 1944 by the M_w 7.4–7.6 Gerede-Bolu earthquake (Figure 1) (Ambraseys, 1970; Barka, 1996;

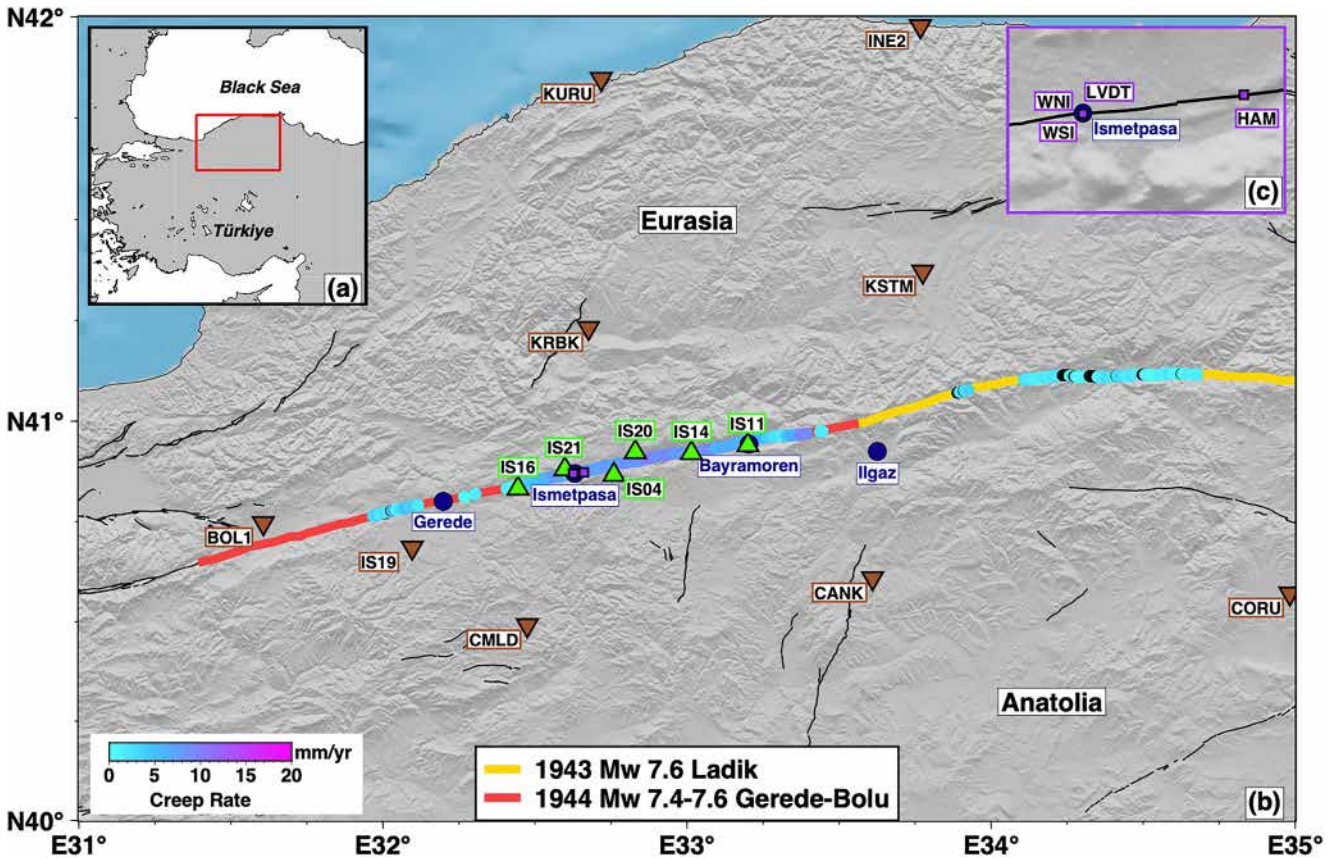

Figure 1. Tectonic setting—(a) Location of the study area in Türkiye. (b) Study area around the central section of the NAFZ. Black lines are active faults (Emre et al., 2018), whereas color-coded dots are surface strike-slip rate measured on InSAR (Jolivet, Jara, Dalaison, et al., 2023). Green triangles are GNSS stations (Jolivet, Jara, & Çakir, 2023), and brown ones are stations from the Turkish National Network. Blue dots are major towns, and purple squares indicate the location of creepmeters around Ismetpasa (local zoom in c). Red and yellow lines show the extent of the 1943 M_w 7.6 Ladik and 1944 M_w 7.4–7.6 Gerede-Bolu earthquakes (Ambraseys, 1970). Gray shaded topography is from SRTM (Farr et al., 2007).

Şengör et al., 2005). Following this event, tens of centimeters of afterslip were reported over the subsequent decade, despite some debate about its amplitude and duration (Ambraseys, 1970; Bilham et al., 2016). Early studies indicated higher surface creep rates along the Ismetpasa segment, but re-analysis suggests that since approximately 1960, the aseismic slip rate has remained relatively constant at 6–7 mm/yr (Jolivet, Jara, Dalaison, et al., 2023) to 1 cm/yr (Bilham et al., 2016), with slight decay within uncertainties. These measurements include various geodetic methods (geodetic triangulation, creepmeter, LIDAR, GNSS and InSAR) (Altay & Sav, 1991; Bilham et al., 2016; Cakir et al., 2005; Cetin et al., 2014; Deniz et al., 1993; Eren, 1984; Jolivet, Jara, Dalaison, et al., 2023; Kaneko et al., 2013; Karabacak et al., 2011; Kutoglu et al., 2008; Ozener et al., 2013). InSAR data also showed that aseismic slip extends 70 km along strike, from 15 km west of Ismetpasa to 15 km east of Bayramoren (Figure 1).

In addition to this long-term aseismic behavior, week-long transient SSEs have been reported around Ismetpasa. Altay and Sav (1991) and Bilham et al. (2016) documented events in 1987 and 2015 with slip ranging from 1.5 to 2.5 mm using creepmeters. Rousset et al. (2016) identified a very shallow SSE (0–4 km depth) in August 2013 lasting 31 days with a magnitude of M_w 5.2–5.5 using InSAR. More recently, Jolivet, Jara, Dalaison et al. (2023) found SSEs near Ismetpasa with a recurrence interval of 2–2.5 years, affecting only the steady creep region's edges. Their study, however, focused on surface slip rates and lacked resolution for time-dependent processes at depth, with InSAR providing 6-day temporal resolution. Here, we analyze creepmeter and GNSS data (Figure 1) to investigate an SSE from late 2019 to early 2020 (Figure 2a). Our approach combines local reference frame definitions with Multichannel Singular Spectrum Analysis (MSSA) to extract and characterize small SSEs from

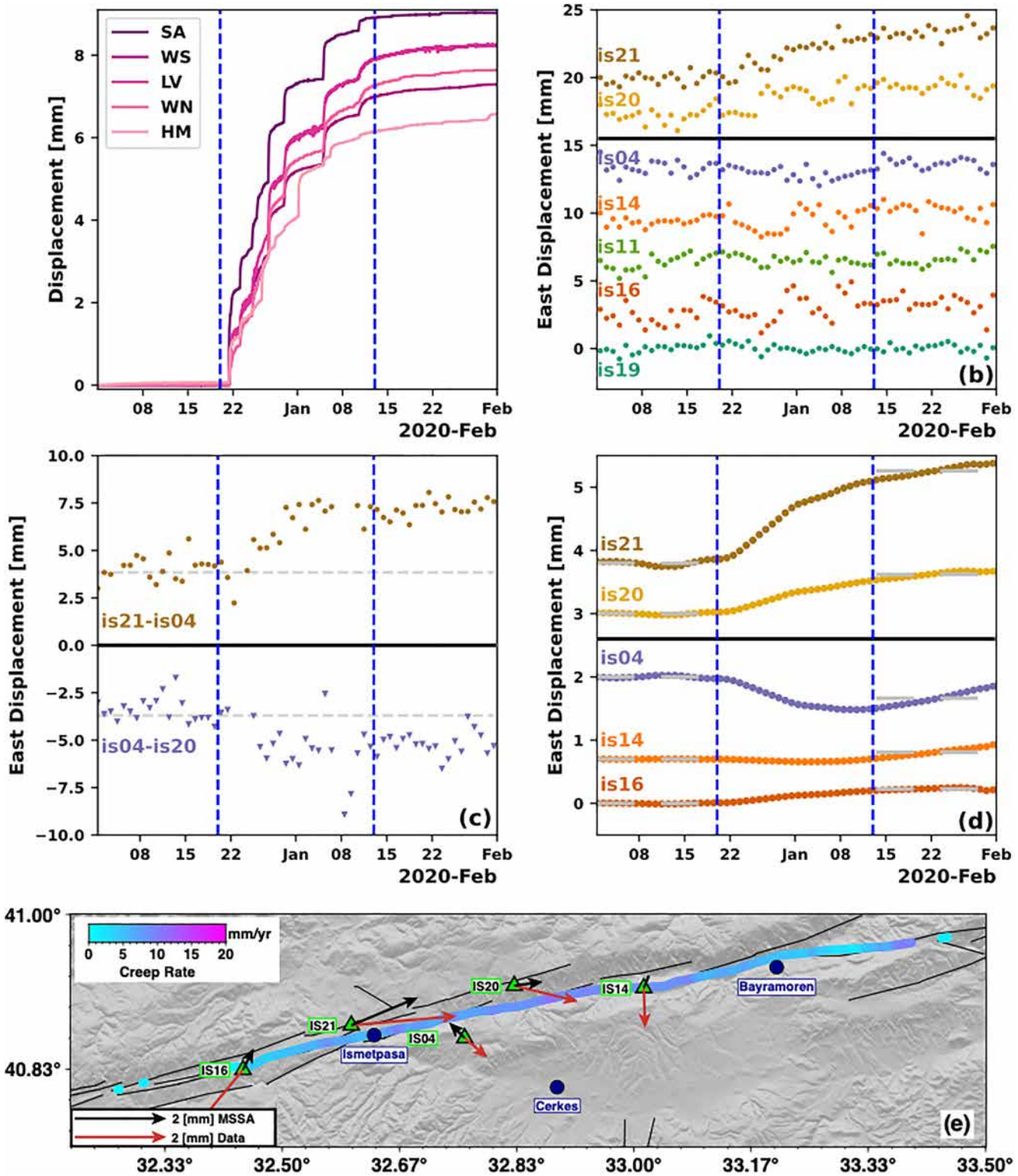

Figure 2. Geodetic observations—(a) Creepmeter displacements near Ismetpasa, color-coded by station (SA: West Sazlik, WN: Wall North, WS: Wall South, HM: Hamamlı, LV: Linear Voltage Transducer). Blue dashed lines indicate the start (21/12/2019) and end (13/01/2020) of the SSE. (b) Raw east-west GNSS displacement for Ismetpasa-area stations, color-coded by name, with a black line separating stations north and south of the fault. (c) East component baseline for station pairs near Ismetpasa. (d) MSSA first component displacement for five stations, with gray dashed lines showing mean displacement pre- and post-SSE. (e) Map view of GNSS displacement (red) and MSSA first component (black), with NAFZ creep rates from Jolivet, Jara, Dalaison, et al. (2023).

noisy GNSS data and compares results with creepmeter observations. We also explore the relationship between SSEs and long-term creep in the NAFZ, discussing potential mechanisms driving aseismic slip in this region.

2. Data, Methods and Results

2.1. Creepmeter Observations and a SSE in December 2019–January 2020

Creepmeters have operated intermittently since the 1980s along the central section of the NAFZ near Ismetpasa (Figure 1) (Altay & Sav, 1991; Bilham et al., 2016). On 21 December 2019, a fault slip event consistent with the expected SSE recurrence interval for this section was detected, corroborated by InSAR observations (Jolivet, Jara, Dalaison, et al., 2023). At 08:46 UTC, the West Sazlik creepmeter recorded increasing extension over 4 minutes, interpreted as strain from an approaching dislocation tip. Surface slip nucleated at 08:50 UTC, followed by at least seven discrete sub-events propagating eastward over 16 days (Figures 1, 2a and Figures S3, S19 in Supporting Information S1). Surface slip reached 7–8 mm at Ismetpasa and 6 mm at Hamamlı, 2–3 km east of Ismetpasa, with maximum cumulative slip at Ismetpasa reaching 9 mm by 6 January 2020. Although no surface slip was detected at the Cerkes creepmeter, 9.75 km to the east, it is likely that surface slip extended farther east beyond the Hamamlı creepmeter.

While creepmeters capture the along-strike extent of small aseismic events, their small aperture (less than 10 m) limits constraints on the depth of slip (Gittins & Hawthorne, 2022). InSAR provides spatial deformation data but often struggles with atmospheric noise, obscuring signals from creep events with less than 1 cm slip (Materna et al., 2024; Rouet-Leduc et al., 2021). To overcome these limitations and characterize the SSE detected by creepmeters and InSAR, we used GNSS time series from the Ismenet network (Jolivet, Jara, & Çakir, 2023), leveraging creepmeter-based timing to refine our analysis.

2.2. GNSS Processing and Time Series Analysis

We use GNSS displacement time series processed by Jolivet, Jara, Dalaison, et al. (2023) (see the Supporting Information S1 for details on the processing (Herring et al., 2018) and associated parameters (Altamimi et al., 2017; Griffiths, 2019; Lyard et al., 2006; Montenbruck et al., 2015; Petit & Luzum, 2013; Tregoning & van Dam, 2005)) to define a local reference frame, following the methodology of Nocquet et al. (2016), to extract small deformation signals. This approach enhances local motion and highlights changes in the geodetic network's shape over time rather than its global motion. Stations with good repeatability and minimal data gaps (BOL1, CANK, CMLD, CORU, INE2, IS19, KRBK, KSTM, KURU, SINP, ZONG; Figure 1, brown triangles) are selected to define the local reference frame, assuming 0 mm/yr velocity at the reference epoch 2020.0. Using PYACS software (Nocquet & Dinh Trong, 2025), we perform an iterative Helmert transform to transition from ITRF to local coordinates, reducing mean Helmert transformation errors from 0.99 mm (east) and 1.30 mm (north) to 0.33 and 0.42 mm, respectively. This procedure transitions from a solution with a millimeter to a sub-millimeter precision, limiting common mode effects and just reflecting changes in the spatial configuration of the network over time and especially any internal deformation (Nocquet et al., 2016). Furthermore, we get a good repeatability for the time series, with values that range from 0.53 to 1.33 mm for the north component and from 0.49 to 1.56 mm for the east component, as detailed in Table S1 and Figure S4 in Supporting Information S1.

During the observation period, six Ismenet stations (green triangles in Figure 1) are active. Stations north of the fault (IS21 and IS20) show 1–2 mm eastward displacement (Figures 2b and 2e), consistent with right-lateral motion detected by creepmeters (Figure 2b, and Figure S3 in Supporting Information S1). No clear right-lateral displacement is observed at southern stations (IS16, IS04, IS14, IS11). Since the reference frame is local, the relative motion between stations on either side of the fault is more relevant than absolute station motion. Hence, we calculate baseline lengths between station pairs to evaluate relative displacement. Stations north of the fault move eastward relative to IS04, south of the fault (Figure 2c). This pattern is evident at IS21, IS04, and IS20, while stations outside this region show minimal displacement (Figure S5 in Supporting Information S1). The ∼2–5 mm offset recorded by GNSS aligns with creepmeters' surface fault slip measurements, confirming an SSE near Ismetpasa. In order to characterize this event, we now need to extract its signature and solve for its depth extent.

2.3. SSE Source Characterization

2.3.1. Multichannel Singular Spectrum Analysis

GNSS time series include various signals, including interseismic and seasonal loading, common mode, earthquakes, SSEs, and noise related to site characteristics and processing. Our analysis indicates that the GNSS time series, within our local reference frame, captured a SSE embedded in geodetic noise. We extract this SSE signal using Multichannel Singular Spectrum Analysis (MSSA) (Walwer et al., 2016), which separates signals with common spatio-temporal patterns from multiple time series without prior knowledge of their amplitude or duration (Groth & Ghil, 2011; Gruszczynska et al., 2018). MSSA uses the covariance matrix of the trajectory matrix, diagonalized using singular-value decomposition, to identify key eigenvalues and eigenvectors (empirical orthogonal functions) that reconstruct the time series, isolating coherent signals across the network (Groth & Ghil, 2011; Walwer et al., 2016; N. K. Voss et al., 2017; Gruszczynska et al., 2018).

MSSA needs continuous time series with no gap. To address this, we perform data-driven gap filling using MSSA. First, gaps are linearly interpolated. Then, MSSA is applied to the north and east components for each station using a 30-day time window (TW). We reconstruct the time series iteratively for 30 iterations, filling gaps based on each station's characteristic noise (Figure S6 in Supporting Information S1 shows gap filling for all stations; Figure S7 in Supporting Information S1 provides an example at station IS14).

Once data gaps are filled, we apply MSSA to the GNSS time series with TWs of 5, 10, 15, 20, 25, and 30 days for stations IS21, IS20, IS16, IS04, and IS14 (Figure 1). The first MSSA component consistently shows transient right-lateral motion across the fault, regardless of the TW chosen (Figure S15c in Supporting Information S1). The choice of TW leads to different amplitudes of the transient signal. We therefore take the mean of this first MSSA component for different TWs, resulting in an effective TW of 10–20 days. These results highlight the occurrence and location of an SSE (Figure 2d), as observed in our baseline analysis (Figure 2c). Stations IS21, IS20, and IS04 show a millimetric to sub-millimetric displacement, while stations IS16 and IS14 (outside the Ismetpasa region) show almost no motion (Figure 2d). Examining the resulting displacement field (Figure 2e, green arrows), we observe that stations IS20 and IS21 (north of the fault) move eastward, with a consistent pattern and amplitude. In contrast, IS04, located south of the fault, moves westward, a pattern not observed in the raw data.

This signal is robust, with displacement amplitude varying by less than 10% when additional GNSS stations are included (Figures S15 and S16 in Supporting Information S1). However, station IS11 exhibits unusual north-component behavior, likely due to the instability of its concrete pillar, which had not fully settled after installation six months before the SSE. Thus, we exclude IS11 from the analysis, focusing on the remaining five stations.

To verify these results, we examine the correlation between MSSA components across different TWs and their contribution to the observed variance (Figure S8 in Supporting Information S1). Typically, three to four MSSA components explain over 80% of the variance. While MSSA components 1 and 2 are uncorrelated, later components (3 and 4) show some correlation patterns. Reconstructing the time series confirms that the first MSSA component aligns well with expected displacement south of the fault, while the second component captures residual common mode not removed during local reference frame definition (Figures S9–S14 in Supporting Information S1). Using up to 10 MSSA components effectively smooths the time series, further supporting our approach (Figures S9–S14 in Supporting Information S1). Our results confirm that the SSE detected by the creepmeter array and InSAR time series (Jolivet, Jara, Dalaison, et al., 2023) is also captured by GNSS stations.

2.3.2. Slip Distribution of the 2019 SSE

We use the cleaned up time series from five stations (Figure 2d and Figure S15 in Supporting Information S1) to estimate the SSE duration, following the approach by Jara et al. (2024). Effectively, we compute a stack of the GNSS displacement time series, weighted by the Green's functions (i.e., surface displacements at the position of each station considering unit slip on each point of the fault) to highlight the duration of the slip event (Jara et al., 2024; Mouchon et al., 2023; Rousset et al., 2019).

To compute the Green's functions, we discretize the North Anatolian fault plane at depth assuming a vertical fault following the trace mapped at the surface according to the geometry proposed by Jolivet, Jara, Dalaison,

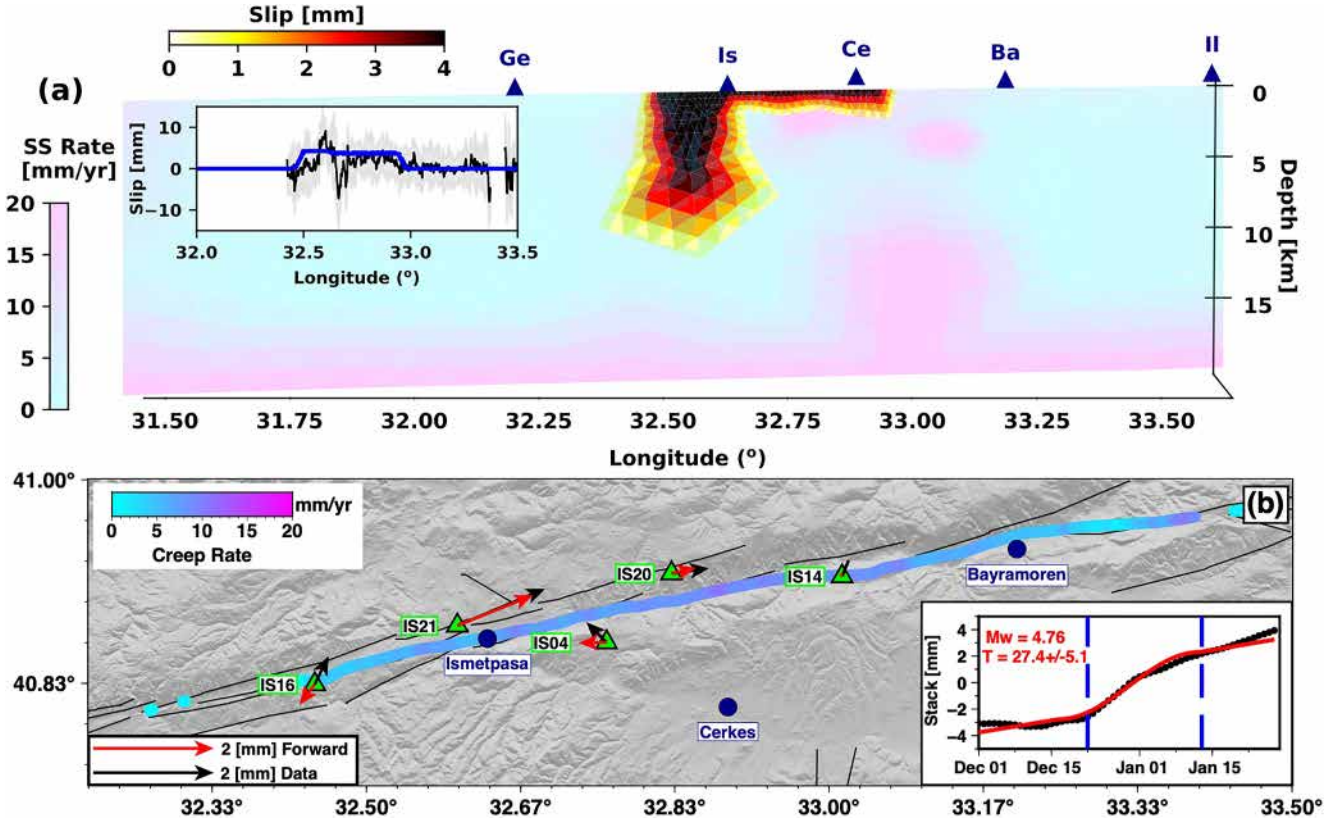

Figure 3. Slip distribution and model performance—(a) SSE slip distribution along the NAFZ central section. Background shows long-term slip rates (Jolivet, Jara, Dalaison, et al., 2023), with locked (light blue) and creeping (pink) regions. Dark blue triangles mark towns along the fault. The inset compares InSAR surface slip (black) with our SSE slip (blue) and associated uncertainties (gray shading). (b) MSSA displacement map (black arrows) with SSE slip model predictions (red arrows). The inset shows the GNSS weighted stack (black dots) and the model used for SSE duration estimation (red line). Blue dashed lines indicate SSE duration from creepmeters.

et al. (2023) in which triangle size varies from 1 km at the surface to 10 km at depth (112 nodes in total). We then evaluate the Green's functions using the EDKS software (Zhu & Rivera, 2002), assuming a stratified elastic medium with elastic parameters taken from Rousset et al. (2016).

We estimate on the weighted stack a linear trend and time-dependent slip evolution, defined as $s(t) = \frac{1}{2}\left(1 - \cos\left(\frac{\pi t}{T}\right)\right)$ (Jara et al., 2024; Rousset et al., 2017, 2019). We apply a Bayesian approach to estimate the trend and T, yielding a SSE duration of 27.4 ± 5.1 days (see Figure 3b for the weighted stack and model estimation). We test different GNSS station configurations to determine the stack, and the duration remains fairly similar (26 ± 5 days, Figure S16 in Supporting Information S1). Considering the estimated uncertainties, this matches well with the 26-day duration observed by the creepmeters (Figure 2).

To evaluate the slip distribution, we cannot perform classic data inversion because we only have 10 data points (five for each GNSS component) and because the original noise level is too high. Therefore, we systematically explore different slip configurations to identify the minimum number of contiguous fault nodes that contribute to the observed displacement (All possible 2048 node configurations made of contiguous nodes around the principal detected node are tested. See Supporting Information S1 for a detailed explanation of the forward modeling approach). On these nodes (Figure S16 in Supporting Information S1), we explore a range of magnitudes (M_w 4.0–5.5) to minimize the RMS between the observations and the model, assuming constant slip on the area affected by slip. We obtain the best fit between the model and observations for a SSE with a magnitude of M_w 4.8 ± 0.08 (Figure 3). This number remains robust regardless of the number of stations included in the estimation (Figure S17 in Supporting Information S1).

The SSE we identify is very shallow (less than 1 km depth) between the villages of Ismetpasa and Cerkes eastwards, while to the west of Ismetpasa, it deepens to a depth of 5–7 km (Figure 3 and Figure S18 in Supporting Information S1). Additionally, surface slip inferred from our slip model aligns with similar measurements inferred from InSAR-derived deformation rates (Figure 3a, inset and Figure S18 in Supporting Information S1) (Jolivet, Jara, Dalaison, et al., 2023).

3. Discussion

3.1. Consistency Between GNSS and Creepmeter Observations

Our results demonstrate strong agreement between slip observed by creepmeters and GNSS stations, particularly in timing and duration (26 ± 5 days). The main differences are in observed displacement and estimated moment-magnitude. Creepmeters recorded a maximum slip of 9 mm during the SSE, while forward modeling using GNSS observations indicates a mean slip of 4.3 mm. However, surface slip measured by creepmeters tapered from 9 to 6 mm along 3.1 km strike to east and was not detected at Cerkes, 10 km east of Sazlik (Figure S3 in Supporting Information S1). Assuming a linear decrease in surface slip of 1 mm/km over 9 km, the average slip would be ∼4.5 mm, closely matching the GNSS-derived value.

A reduction in slip with depth is also expected for a creep event intersecting the free surface of an elastic half-space. This suggests that GNSS estimates represent spatially averaged slip, whereas creepmeters provide localized point measurements. Larger surface slip values recorded by creepmeters are consistent with the increase in secular creep rates from zero at ∼3 km depth to a maximum at the surface (Bilham et al., 2016). Therefore, the moment-magnitude estimated from GNSS observations (M_w 4.8 ± 0.08) is more representative of this SSE than the magnitude derived from the maximum local slip measured by the creepmeters (M_w 5.0).

The creepmeter array records eastward propagation of the slow slip event, encompassing the initial surface slip and six subsequent sub-events that incrementally complete the slip (Figure S3 in Supporting Information S1). Slip starts at 08.46 UTC on 21/12/2019 at Sazlik (Figure S19a in Supporting Information S1) with rapid fault slip rate starting at 08.50 UTC. Maximum slip velocities are observed 7 min later at the three Ismetpasa off-set wall sensors, located 540 m to the west, and 26 min later at Hamamlı, 3.13 km further east (Figures S3 and S19a–S19c in Supporting Information S1). Eastward propagation velocities for sub-events (Figure S3 in Supporting Information S1) across the four creepmeter locations range from 0.3 m/s to 2.3 m/s. This migration pattern is not captured by the GNSS observations (Figures 2b and 2c). However, MSSA components used to characterize the SSE indicate a change in slip speed around 1 January 2020 (Figure 2d). Both results suggest temporal complexity in the SSE source, which our forward modeling approach cannot capture.

Simultaneous observations of SSEs by GNSS and creepmeters have been documented at several fault systems, including the San Andreas (Michel et al., 2022), Imperial Valley (Materna et al., 2024), and Superstition Hills (Vavra et al., 2024) faults. The observed fault slip in these studies amounted 10–30 mm (creepmeters and GNSS). Resolving sub-centimeter slip at depth on a creeping fault using GNSS requires sub-millimeter noise levels in measurements flanking the fault. Our approach shows that sub-mm signal-to noise measurements are indeed attainable with GNSS methods. Moreover, our observations confirm that the fault slip recorded by creepmeters along this section of the NAFZ is not limited to very shallow depths but extends into the first kilometers of the crust. This finding provides valuable insights into fault mechanics and helps bridge an observational gap, particularly in estimating moment-magnitude scaling laws (Ide & Beroza, 2023; Materna et al., 2024).

3.2. Mechanism Driving the SSE

No earthquakes nor quarry blasts are reported by Turkish agencies AFAD (https://deprem.afad.gov.tr/event-catalog, last accessed on 07/07/2024) and KOERI (http://www.koeri.boun.edu.tr/sismo/2/earthquake-catalog, last accessed on 07/07/2024) in the area during the period 01/12/2019–01/02/2020. We also explore the International Seismological Center catalog for 21/12/2019 (International Seismological Centre, 2024) between 07:00 and 12:00 UTC (last accessed on 07/07/2024), finding no earthquakes above magnitude 4.5 at a teleseismic distance. Then, failure was not triggered by dynamic strain associated with transient surface waves (Bilham & Castillo, 2020). However, we do not rule out the possibility that microseismicity, not captured by regional networks, might trigger a seismic/aseismic interaction, where afterslip from seismic activity could trigger the SSE, as

suggested in the western section of the NAFZ (Martínez-Garzón et al., 2019, 2021), with magnitudes comparable to our event.

We observe a significant change in atmospheric pressure associated with an approaching storm front near Ismetpasa. Atmospheric pressure peaked on 20 December and dropped sharply 4 days later (∼2 kPa). A barometer and rain gauge at the Ismetpasa creepmeter recorded heavy rainfall beginning around midday on 23 December, followed by a pressure minimum below 890 mb early on 24 December (Figure S3 in Supporting Information S1). Since these events (surface loading from rainfall and barometric surface unloading) occurred many hours after surface slip had already commenced, they cannot have directly triggered the slip. However, barometric unloading due to the approaching storm front would have resulted in surface strain and tilts before the arrival of both the rain and pressure events. Similar observations have been reported in Taiwan, where pressure drops associated with typhoons (2–4 kPa) have been shown to induce Coulomb stress changes and trigger SSEs along faults (Liu et al., 2009; Mouyen et al., 2017). Therefore, we hypothesize that the Coulomb failure changes caused by these loading effects may have contributed to triggering the accumulated shallow-slip deficit, although a detailed quantitative discussion of this triggering mechanism is beyond the scope of the present article.

The eastward migration pattern detected by the creepmeters (Figure S19 in Supporting Information S1) suggests that the 2019 SSE nucleated west of Ismetpasa, where deeper slip is required to fit the observations at GNSS station IS21 (Figure 3b). This region corresponds to a transitional slip rate zone (10 mm/yr, Figure S18a in Supporting Information S1) (Cetin et al., 2014; Jolivet, Jara, Dalaison, et al., 2023), which aligns with proposed SSE-hosting areas characterized by transitional geodetic interseismic coupling (Avouac, 2015; Bürgmann, 2018; Jara et al., 2024; Jolivet & Frank, 2020; Mazzotti et al., 2000). By analyzing small slip events hidden in geodetic noise, this idea has been corroborated with observations from many subduction zones worldwide (Frank, 2016; Jara et al., 2024; Materna et al., 2019) and more recently along continental strike-slip faults (Materna et al., 2024; Michel et al., 2022; Vavra et al., 2024). Our results suggest that this apparent transitional slip rate might be due to multiple SSEs accumulated during the observational period, as detected by InSAR (Jolivet, Jara, Dalaison, et al., 2023) and creepmeter (Bilham et al., 2016) observations.

East of Ismetpasa, our forward model shows that slip is confined to shallower depths (less than 2 km, Figure 3a), as no deep slip is required to fit the GNSS observations. Here, the fault slip rate ranges from 6 to 10 mm/yr, half of the velocity inferred between 2 and 8 km depth. We observe that no slip extends into the long-term creeping section at depth, stopping near GNSS station IS20 (Figure 3). No SSEs have been detected thus far within the steady-state creep region (extending eastward from Cerkes to Bayramoren, Figure 3a) using either GNSS or InSAR observations (Jolivet, Jara, Dalaison, et al., 2023). However, shallow SSEs (0–4 km) have been detected in the area using InSAR observations, with similar slip patterns to those presented in this work. Rousset et al. (2016) reported an SSE in mid-2013, and Jolivet, Jara, Dalaison, et al. (2023) also reported surface slip variations along-strike in 2017 and during the event we report in this study, with similar along-strike extents compared to our results, suggesting a recurrence time of 2–3 years (Bilham et al., 2016; Jolivet, Jara, Dalaison, et al., 2023). Our main contribution is that we provide evidence that the two types of aseismic slip seem to coexist in the area. On one hand, we observe burst-like behavior beneath Ismetpasa between the surface and a depth of 5 km, extending up to 20 km eastward at 0–2 km-depth. On the other hand, we observe a section constantly slipping at 2 cm/yr (2–10 km depth) over the observation period (Bilham et al., 2016; Jolivet, Jara, Dalaison, et al., 2023). This result confirms that aseismic slip rates reported over many years with observations made at Ismetpasa (GNSS, creepmeters, LIDAR, and geodetic triangulations) (Altay & Sav, 1991; Bilham et al., 2016; Deniz et al., 1993; Eren, 1984; Karabacak et al., 2011; Kutoglu et al., 2008; Ozener et al., 2013) are not fully representative of the aseismic slip behavior in the entire area. Moreover, our results suggest that transitional slip rate values estimated using InSAR observations (Cetin et al., 2014; Jolivet, Jara, Dalaison, et al., 2023; Kaneko et al., 2013) might represent regions that transiently release stress via SSEs.

We hypothesize that SSEs in Ismetpasa occur because the zone is elastically loaded by the adjacent steady-state creeping section. Considering that there are no residual afterslip effects from past earthquakes in the area (Bilham et al., 2016; Jolivet, Jara, Dalaison, et al., 2023), we can estimate elastic stress increase during the interseismic period imposed by constant slip on the creeping section. If the steadily creeping zone slides at 1.5–2.0 cm/yr and if each SSEs releases 4–8 mm, the recurrence time of these events is between 2 and 5 years. This recurrence time is consistent with observations from creepmeters (Bilham et al., 2016) and InSAR (Jolivet, Jara, Dalaison, et al., 2023; Rousset et al., 2016); however, longer observations are required to confirm this recurrence. On a

yearly scale, Murray and Segall (2005) observe a complex mix of seismic and aseismic interactions at Parkfield (California, US) using geodetic data (electronic distance meters, creepmeters, and strainmeters). Their results suggest that the creep zone of the San Andreas Fault could trigger moderate magnitude seismicity (M_w 4–5), and its associated afterslip could trigger a long-lived SSE. Similar results have been observed in the western part of the NAFZ (Armutlu Peninsula), but on a monthly scale. Relocated seismic catalogs show that earthquakes of magnitude 3–4 trigger afterslip. A comparison of these results with strainmeter observations suggests that afterslip might trigger an SSE with a duration of approximately 50–60 days (Martínez-Garzón et al., 2019, 2021). In our case, as mentioned above, no seismicity is reported in the study area, suggesting that the SSEs are mainly aseismic and not triggered by afterslip. This supports our hypothesis that the steadily creeping zone is responsible for the loading and spontaneous occurrence of the SSEs, which is supported by numerical models of aseismic slip and seismic cycling (Bruhat, 2019; Perfettini & Ampuero, 2008).

4. Conclusions

We analyze fault slip behavior along the central section of the NAFZ, using geodetic observations from GNSS and creepmeters, a local reference frame definition, and time series analysis. Our approach demonstrates the effectiveness of MSSA in extracting transient signals from noisy GNSS observations, supported by its good agreement with creepmeter data. We identify a slow slip event (SSE) that occurred between December 2019 and January 2020, with a duration of 26 ± 5 days and an equivalent moment-magnitude of M_w 4.8 ± 0.08.

We detected a SSE, that we interpret to be nucleated on a ∼5 km × 5 km deep subsurface patch of the fault to the west of the surface creepmeters at Ismetpasa, and to have propagated eastward as a shallow (< 2 km) deep creep event. By comparing our SSE slip model with previous studies in the area (Cetin et al., 2014; Jolivet, Jara, Dalaison, et al., 2023), we find that aseismic slip in the region is characterized by two behaviors: burst-like SSEs every 2–5 years and steady-state creep. We show that our SSE has a tectonic origin, is primarily aseismic, and is unrelated to seismic activity, though atmospheric pressure changes may have contributed to its triggering. We hypothesize that the steadily creeping section (eastward from Ismetpasa to Bayramoren, long-term slip rate in Figure 3a) nearby loads the area over which our SSE occurred near Ismetpasa, with a potential recurrence interval of 2–5 years. Our findings provide a high-resolution description of fault behavior and illustrate how different aseismic slip behaviors interact throughout the seismic cycle. Additionally, they help fill the observational gap widely discussed in moment-duration scaling laws (Ide & Beroza, 2023; Materna et al., 2024).

Data Availability Statement

GNSS observations from IGS and the Turkish National GNSS network are available at http://www.igs.org and https://www.tusaga-aktif.gov.tr. Ismenet observations can be retrieved from (Jolivet, Jara, & Çakir, 2023). Creepmeter data are publicly available via GAGE (formerly UNAVCO) facility https://www.unavco.org/data/strain-seismic/creep-data/creep-data.html. Reference frame definition and iteration are performed using PYACS software (Nocquet & Dinh Trong, 2025) (https://github.com/JMNocquet/pyacs36). Forward modeling and Green's function calculation are carried out using the Classical Slip Inversion library (Jolivet, 2024) (https://github.com/jolivetr/csi). All calculations are done using Python 3.11 (Van Rossum & Drake, 2009) and the packages MSSA (https://github.com/kieferk/pymssa) and PyMC (Abril-Pla et al., 2023). All plots are made using Matplotlib (Hunter, 2007) and PyGMT (Tian et al., 2024).

Acknowledgments
This work is dedicated to the memory of Muhtar Satılmış Üke, whose support was crucial for the installation and maintenance of the Ismenet network. J. Jara acknowledges the support of a MSCA Individual Fellowship from the European Union's Horizon 2020 (ERASMUS, No. 101066069). R. Jolivet acknowledge funding from the European Research Council (ERC) under Horizon 2020 (Grant agreement 758210, project Geo4D). R. Bilham acknowledges NSF Award EAR 2318733 for supporting creepmeter measurements.

References

Abril-Pla, O., Andreani, V., Carroll, C., Dong, L., Fonnesbeck, C. J., Kochurov, M., et al. (2023). PyMC: A modern, and comprehensive probabilistic programming framework in Python. *PeerJ Computer Science*, *9*, e1516. https://doi.org/10.7717/peerj-cs.1516

Altamimi, Z., Métivier, L., Rebischung, P., Rouby, H., & Collilieux, X. (2017). ITRF2014 plate motion model. *Geophysical Journal International*, *209*(3), 1906–1912. https://doi.org/10.1093/gji/ggx136

Altay, C., & Sav, H. (1991). Continuous creep measurement along the North Anatolian Fault Zone. *Bulletin of the Geological Congress of Turkey*, *6*, 77–81.

Ambraseys, N. (1970). Some characteristic features of the Anatolian fault zone. *Tectonophysics*, *9*(2–3), 143–165. https://doi.org/10.1016/0040-1951(70)90014-4

Avouac, J.-P. (2015). From geodetic imaging of seismic and aseismic fault slip to dynamic modeling of the seismic cycle. *Annual Review of Earth and Planetary Sciences*, *43*(1), 233–271. https://doi.org/10.1146/annurev-earth-060614-105302

Barka, A. (1996). Slip distribution along the North Anatolian fault associated with the large earthquakes of the period 1939 to 1967. *Bulletin of the Seismological Society of America*, *86*(5), 1238–1254. https://doi.org/10.1785/bssa0860051238

Bilham, R., & Castillo, B. (2020). The July 2019 ridgecrest, California, earthquake sequence recorded by creepmeters: Negligible epicentral afterslip and prolonged triggered slip at teleseismic distances. *Seismological Research Letters*, *91*(2A), 707–720. https://doi.org/10.1785/0220190293

Bilham, R., Ozener, H., Mencin, D., Dogru, A., Ergintav, S., Cakir, Z., et al. (2016). Surface creep on the North Anatolian Fault at Ismetpasa, Turkey, 1944-2016. *Journal of Geophysical Research: Solid Earth*, *121*(10), 7409–7431. https://doi.org/10.1002/2016JB013394

Bruhat, L. (2019). A physics-based approach of deep interseismic creep for viscoelastic strike-slip earthquake cycle models. *Geophysical Journal International*, *220*(1), 79–95. https://doi.org/10.1093/gji/ggz426

Bürgmann, R. (2018). The geophysics, geology and mechanics of slow fault slip. *Earth and Planetary Science Letters*, *495*, 112–134. https://doi.org/10.1016/j.epsl.2018.04.062

Bürgmann, R., Kogan, M. G., Levin, V. E., Scholz, C. H., King, R. W., & Steblov, G. M. (2001). Rapid aseismic moment release following the 5 December, 1997 Kronotsky, Kamchatka, earthquake. *Geophysical Research Letters*, *28*(7), 1331–1334. https://doi.org/10.1029/2000GL012350

Bürgmann, R., Kogan, M. G., Steblov, G. M., Hilley, G., Levin, V. E., & Apel, E. (2005). Interseismic coupling and asperity distribution along the Kamchatka subduction zone. *Journal of Geophysical Research*, *110*(7), 1–17. https://doi.org/10.1029/2005JB003648

Cakir, Z., Akoglu, A., Belabbes, S., Ergintav, S., & Meghraoui, M. (2005). Creeping along the Ismetpasa section of the North Anatolian fault (Western Turkey): Rate and extent from InSAR. *Earth and Planetary Science Letters*, *238*(1–2), 225–234. https://doi.org/10.1016/j.epsl.2005.06.044

Cetin, E., Cakir, Z., Meghraoui, M., Ergintav, S., & Akoglu, A. M. (2014). Extent and distribution of aseismic slip on the Ismetpaşa segment of the North Anatolian Fault (Turkey) from persistent scatterer InSAR. *Geochemistry, Geophysics, Geosystems*, *15*(7), 2883–2894. https://doi.org/10.1002/2014GC005307

Dalaison, M., Jolivet, R., van Rijsingen, E. M., & Michel, S. (2021). The interplay between seismic and aseismic slip along the chaman fault illuminated by InSAR. *Journal of Geophysical Research: Solid Earth*, *126*(12), 1–23. https://doi.org/10.1029/2021JB021935

Deniz, R., Aksoy, A., Yalin, D., Seeger, H., Franke, P., Hirsch, O., & Bautsch, P. (1993). Determination of crustal movements in Turkey by terrestrial geodetic methods. *Journal of Geodynamics*, *18*(1–4), 13–22. https://doi.org/10.1016/0264-3707(93)90024-Z

Emre, O., Duman, T. Y., Özalp, S., Şaroğlu, F., Olgun, S., Elmacı, H., & Çan, T. (2018). Active fault database of Turkey. *Bulletin of Earthquake Engineering*, *16*(8), 3229–3275. https://doi.org/10.1007/s10518-016-0041-2

Eren, K. (1984). Strain analysis along the North Analtolian Fault by using geodetic surveys. *Bulletin Geodesique*, *58*(2), 137–150. https://doi.org/10.1007/BF02520898

Farr, T. G., Rosen, P. A., Caro, E., Crippen, R., Duren, R., Hensley, S., et al. (2007). The shuttle radar topography mission. *Reviews of Geophysics*, *45*(2), RG2004. https://doi.org/10.1029/2005RG000183

Frank, W. B. (2016). Slow slip hidden in the noise: The intermittence of tectonic release. *Geophysical Research Letters*, *43*(19), 10125–10133. https://doi.org/10.1002/2016GL069537

Gittins, D. B., & Hawthorne, J. C. (2022). Are creep events big? Estimations of along-strike rupture lengths. *Journal of Geophysical Research: Solid Earth*, *127*(1), 1–26. https://doi.org/10.1029/2021JB023001

Griffiths, J. (2019). Combined orbits and clocks from IGS second reprocessing. *Journal of Geodesy*, *93*(2), 177–195. https://doi.org/10.1007/s00190-018-1149-8

Groth, A., & Ghil, M. (2011). Multivariate singular spectrum analysis and the road to phase synchronization. *Physical Review E - Statistical, Nonlinear and Soft Matter Physics*, *84*(3), 1–10. https://doi.org/10.1103/PhysRevE.84.036206

Gruszczynska, M., Rosat, S., Klos, A., Gruszczynski, M., & Bogusz, J. (2018). Multichannel singular spectrum analysis in the estimates of common environmental effects affecting GPS observations. *Pure and Applied Geophysics*, *175*(5), 1805–1822. https://doi.org/10.1007/s00024-018-1814-0

Heki, K., Miyazaki, S., & Tsuji, H. (1997). Silent fault slip following an interplate thrust earthquake at the Japan Trench. *Nature*, *386*(6625), 595–598. https://doi.org/10.1038/386595a0

Herring, T., King, R., Floyd, M., & McClusky, S. (2018). Introduction to GAMIT/GLOBK, release 10.7.

Hsu, Y.-J., Bechor, N., Segall, P., Yu, S.-B., Kuo, L.-C., & Ma, K.-F. (2002). Rapid afterslip following the 1999 Chi-Chi, Taiwan Earthquake. *Geophysical Research Letters*, *29*(16), 1–4. https://doi.org/10.1029/2002GL014967

Hunter, J. D. (2007). Matplotlib: A 2D graphics environment. *Computing in Science & Engineering*, *9*(3), 90–95. https://doi.org/10.1109/MCSE.2007.55

Ide, S., & Beroza, G. C. (2023). Slow earthquake scaling reconsidered as a boundary between distinct modes of rupture propagation. *Proceedings of the National Academy of Sciences*, *120*(32), 2017. https://doi.org/10.1073/pnas.2222102120

International Seismological Centre. (2024). *On-line Bulletin*. https://doi.org/10.31905/D808B830

Jara, J., Jolivet, R., Socquet, A., Comte, D., & Norabuena, E. (2024). Detection of slow slip events along the southern Peru - Northern Chile subduction zone. *Seismica*, *3*(1). https://doi.org/10.26443/seismica.v3i1.980

Jara, J., Socquet, A., Marsan, D., & Bouchon, M. (2017). Long-term interactions between intermediate depth and shallow seismicity in North Chile subduction zone. *Geophysical Research Letters*, *44*(18), 9283–9292. https://doi.org/10.1002/2017GL075029

Jolivet, R. (2024). CSI: First release [Software]. *Zenodo*. https://doi.org/10.5281/zenodo.14170822

Jolivet, R., Candela, T., Lasserre, C., Renard, F., Klinger, Y., & Doin, M. P. (2015). The burst-like behavior of aseismic slip on a rough fault: The creeping section of the Haiyuan fault, China. *Bulletin of the Seismological Society of America*, *105*(1), 480–488. https://doi.org/10.1785/0120140237

Jolivet, R., & Frank, W. B. (2020). The transient and intermittent nature of slow slip. *AGU Advances*, *1*(1), e2019AV000126. https://doi.org/10.1029/2019AV000126

Jolivet, R., Jara, J., & Çakir, Z. (2023a). The Ismenet network [Dataset]. *OSF*. https://doi.org/10.17605/OSF.IO/9T3N7

Jolivet, R., Jara, J., Dalaison, M., Rouet-Leduc, B., Özdemir, A., Dogan, U., et al. (2023b). Daily to centennial behavior of aseismic slip along the central section of the North Anatolian Fault. *Journal of Geophysical Research: Solid Earth*, *128*(7), 1–35. https://doi.org/10.1029/2022JB026018

Kaneko, Y., Fialko, Y., Sandwell, D. T., Tong, X., & Furuya, M. (2013). Interseismic deformation and creep along the central section of the North Anatolian Fault (Turkey): InSAR observations and implications for rate-and-state friction properties. *Journal of Geophysical Research: Solid Earth*, *118*(1), 316–331. https://doi.org/10.1029/2012JB009661

Karabacak, V., Altunel, E., & Cakir, Z. (2011). Monitoring aseismic surface creep along the North Anatolian Fault (Turkey) using ground-based LIDAR. *Earth and Planetary Science Letters*, *304*(1–2), 64–70. https://doi.org/10.1016/j.epsl.2011.01.017

Kutoglu, H. S., Akcin, H., Kemaldere, H., & Gormus, K. S. (2008). Triggered creep rate on the Ismetpasa segment of the North Anatolian Fault. *Natural Hazards and Earth System Sciences*, *8*(6), 1369–1373. https://doi.org/10.5194/nhess-8-1369-2008

Liu, C., Linde, A. T., & Sacks, I. S. (2009). Slow earthquakes triggered by typhoons. *Nature*, *459*(7248), 833–836. https://doi.org/10.1038/nature08042

Louderback, G. D. (1942). Faults and earthquakes. *Bulletin of the Seismological Society of America*, *32*(4), 305–330. https://doi.org/10.1785/BSSA0320040305

Lyard, F., Lefevre, F., Letellier, T., & Francis, O. (2006). Modelling the global ocean tides: Modern insights from FES2004. *Ocean Dynamics*, *56*(5–6), 394–415. https://doi.org/10.1007/s10236-006-0086-x

Martínez-Garzón, P., Bohnhoff, M., Mencin, D., Kwiatek, G., Dresen, G., Hodgkinson, K., et al. (2019). Slow strain release along the eastern Marmara region offshore Istanbul in conjunction with enhanced local seismic moment release. *Earth and Planetary Science Letters*, *510*, 209–218. https://doi.org/10.1016/j.epsl.2019.01.001

Martínez-Garzón, P., Durand, V., Bentz, S., Kwiatek, G., Dresen, G., Turkmen, T., et al. (2021). Near-fault monitoring reveals combined seismic and slow activation of a fault branch within the istanbul-marmara seismic gap in northwest Turkey. *Seismological Research Letters*, *92*(6), 3743–3756. https://doi.org/10.1785/0220210047

Materna, K., Bartlow, N., Wech, A., Williams, C., & Bürgmann, R. (2019). Dynamically triggered changes of plate interface coupling in southern Cascadia. *Geophysical Research Letters*, *46*(22), 12890–12899. https://doi.org/10.1029/2019GL084395

Materna, K., Bürgmann, R., Lindsay, D., Bilham, R., Herring, T., Crowell, B., & Szeliga, W. (2024). Shallow slow slip events in the Imperial Valley with along-strike propagation. *Geophysical Research Letters*, *51*(12). https://doi.org/10.1029/2023GL108089

Mazzotti, S. S., Le Pichon, X., Henry, P., & Miyazaki, S.-I. (2000). Full interseismic locking of the Nankai and Japan-west Kurile subduction zones: An analysis of uniform elastic strain accumulation in Japan constrained by permanent GPS. *Journal of Geophysical Research*, *105*(B6), 13159–13177. https://doi.org/10.1029/2000jb900060

Michel, S., Jolivet, R., Lengliné, O., Gualandi, A., Larochelle, S., & Gardonio, B. (2022). Searching for transient slow slips along the San Andreas Fault near Parkfield using independent component analysis. *Journal of Geophysical Research: Solid Earth*, *127*(6), 1–19. https://doi.org/10.1029/2021JB023201

Montenbruck, O., Schmid, R., Mercier, F., Steigenberger, P., Noll, C., Fatkulin, R., et al. (2015). GNSS satellite geometry and attitude models. *Advances in Space Research*, *56*(6), 1015–1029. https://doi.org/10.1016/j.asr.2015.06.019

Mouchon, C., Frank, W. B., Radiguet, M., Poli, P., & Cotte, N. (2023). Subdaily slow fault slip dynamics captured by low-frequency earthquakes. *AGU Advances*, *4*(4), 1–15. https://doi.org/10.1029/2022AV000848

Mouyen, M., Canitano, A., Chao, B. F., Hsu, Y., Steer, P., Longuevergne, L., & Boy, J. (2017). Typhoon-induced ground deformation. *Geophysical Research Letters*, *44*(21), 004–011. https://doi.org/10.1002/2017GL075615

Murray, J. R., & Segall, P. (2005). Spatiotemporal evolution of a transient slip event on the San Andreas fault near Parkfield, California. *Journal of Geophysical Research*, *110*(B9), B09407. https://doi.org/10.1029/2005JB003651

Nocquet, J. M., & Dinh Trong, T. (2025). Pyacs: Python tools for geodetic time series and GNSS velocity field analysis [Software]. *Zenodo*. https://doi.org/10.5281/zenodo.14959022

Nocquet, J. M., Sue, C., Walpersdorf, A., Tran, T., Lenôtre, N., Vernant, P., et al. (2016). Present-day uplift of the western Alps. *Scientific Reports*, *6*(June), 1–6. https://doi.org/10.1038/srep28404

Ozener, H., Dogru, A., & Turgut, B. (2013). Quantifying aseismic creep on the Ismetpasa segment of the North Anatolian Fault Zone (Turkey) by 6 years of GPS observations. *Journal of Geodynamics*, *67*, 72–77. https://doi.org/10.1016/j.jog.2012.08.002

Perfettini, H., & Ampuero, J. P. (2008). Dynamics of a velocity strengthening fault region: Implications for slow earthquakes and postseismic slip. *Journal of Geophysical Research*, *113*(9), B09411. https://doi.org/10.1029/2007JB005398

Petit, G., & Luzum, B. (2013). The 2010 reference edition of the IERS conventions. In (pp. 57–61). https://doi.org/10.1007/978-3-642-32998-2{_}10

Radiguet, M., Perfettini, H., Cotte, N., Gualandi, A., Valette, B., Kostoglodov, V., et al. (2016). Triggering of the 2014 Mw7.3 Papanoa earthquake by a slow slip event in Guerrero, Mexico. *Nature Geoscience*, *9*(11), 829–833. https://doi.org/10.1038/ngeo2817

Reid, H. F. (1910). The mechanism of the earthquake. Tech. Rep. In *The California earthquake of April 18, 1906: Rep. Of the state investigation commiss* (Vol. 2, p. 1). Carnegie Institution.

Rouet-Leduc, B., Jolivet, R., Dalaison, M., Johnson, P. A., & Hulbert, C. (2021). Autonomous extraction of millimeter-scale deformation in InSAR time series using deep learning. *Nature Communications*, *12*(1), 6480. https://doi.org/10.1038/s41467-021-26254-3

Rousset, B., Bürgmann, R., & Campillo, M. (2019). Slow slip events in the roots of the San Andreas fault. *Science Advances*, *5*(2), eaav3274. https://doi.org/10.1126/sciadv.aav3274

Rousset, B., Campillo, M., Lasserre, C., Frank, W. B., Cotte, N., Walpersdorf, A., et al. (2017). A geodetic matched filter search for slow slip with application to the Mexico subduction zone. *Journal of Geophysical Research: Solid Earth*, *122*(12), 10498–10514. https://doi.org/10.1002/2017JB014448

Rousset, B., Jolivet, R., Simons, M., Lasserre, C., Riel, B., Milillo, P., et al. (2016). An aseismic slip transient on the North Anatolian Fault. *Geophysical Research Letters*, *43*(7), 3254–3262. https://doi.org/10.1002/2016GL068250

Ruiz, S., Metois, M., Fuenzalida, A., Ruiz, J., Leyton, F., Grandin, R., et al. (2014). Intense foreshocks and a slow slip event preceded the 2014 Iquique Mw8.1 earthquake. *Science*, *345*(6201), 1165–1169. https://doi.org/10.1126/science.1256074

Schurr, B., Asch, G., Hainzl, S., Bedford, J., Hoechner, A., Palo, M., et al. (2014). Gradual unlocking of plate boundary controlled initiation of the 2014 Iquique earthquake. *Nature*, *512*(7514), 299–302. https://doi.org/10.1038/nature13681

Şengör, A. M., Tüysüz, O., Imren, C., Sakinç, M., Eyidoğan, H., Görür, N., et al. (2005). The North Anatolian Fault: A new look. *Annual Review of Earth and Planetary Sciences*, *33*(1), 37–112. https://doi.org/10.1146/annurev.earth.32.101802.120415

Socquet, A., Valdes, J. P., Jara, J., Cotton, F., Walpersdorf, A., Cotte, N., et al. (2017). An 8 Month slow slip event triggers progressive nucleation of the 2014 Chile megathrust. *Geophysical Research Letters*, *44*(9), 4046–4053. https://doi.org/10.1002/2017GL073023

Steinbrugge, K. V., Zacher, E. G., Tocher, D., Whitten, C. A., & Claire, C. N. (1960). Creep on the San Andreas Fault. *Bulletin of the Seismological Society of America*, *50*(3), 389–415. https://doi.org/10.1785/bssa0500030389

Tian, D., Uieda, L., Leong, W. J., Fröhlich, Y., Schlitzer, W., Grund, M., et al. (2024). PyGMT: A Python interface for the generic mapping tools [Software]. *Zenodo*. https://doi.org/10.5281/zenodo.11062720

Tregoning, P., & van Dam, T. (2005). Atmospheric pressure loading corrections applied to GPS data at the observation level. *Geophysical Research Letters*, *32*(22), 1–4. https://doi.org/10.1029/2005GL024104

Van Rossum, G., & Drake, F. L. (2009). Python 3 reference manual [Software]. *CreateSpace*. Retrieved from www.python.org

Vavra, E. J., Fialko, Y., Rockwell, T., Bilham, R., Štěpančíková, P., Stemberk, J., et al. (2024). Characteristic slow-slip events on the superstition Hills Fault, Southern California. *Geophysical Research Letters*, *51*(12), e2023GL107244. https://doi.org/10.1029/2023GL107244

Voss, N., Dixon, T. H., Liu, Z., Malservisi, R., Protti, M., & Schwartz, S. (2018). Do slow slip events trigger large and great megathrust earthquakes? *Science Advances*, *4*(10), eaat8472. https://doi.org/10.1126/sciadv.aat8472

Voss, N. K., Malservisi, R., Dixon, T. H., & Protti, M. (2017). Slow slip events in the early part of the earthquake cycle. *Journal of Geophysical Research: Solid Earth*, *122*(8), 6773–6786. https://doi.org/10.1002/2016JB013741

Walwer, D., Calais, E., & Ghil, M. (2016). Data-adaptive detection of transient deformation in geodetic networks. *Journal of Geophysical Research: Solid Earth*, *121*(3), 2129–2152. https://doi.org/10.1002/2015JB012424

Zhu, L., & Rivera, L. A. (2002). A note on the dynamic and static displacements from a point source in multilayered media. *Geophysical Journal International*, *148*(3), 619–627. https://doi.org/10.1046/j.1365-246X.2002.01610.x